Materials and Design 30 (2009) 609–616

Contents lists available at ScienceDirect

Materials and Design

journal homepage: www.elsevier.com/locate/matdes

Effect of welding parameters on mechanical and microstructural properties of dissimilar AA6082–AA2024 joints produced by friction stir welding

P. Cavaliere [a,*], A. De Santis [a], F. Panella [a], A. Squillace [b]

[a] Department of "Ingegneria dell'Innovazione", Engineering Faculty, University of Salento, Via per Arnesano, I-73100 Lecce, Italy
[b] Department of Materials and Production Engineering, Engineering Faculty, University of Naples "Federico II", I-80125 Naples, Italy

ARTICLE INFO

Article history:
Received 18 May 2007
Accepted 22 May 2008
Available online 21 July 2008

Keywords:
Friction stir welding
Dissimilar joining
Fatigue

ABSTRACT

The effect of processing parameters on the mechanical and microstructural properties of dissimilar AA6082–AA2024 joints produced by friction stir welding was analysed in this study. Different samples were produced by varying the advancing speeds of the tool as 80 and 115 mm/min and by varying the alloy positioned on the advancing side of the tool. In all the experiments the rotating speed is fixed at 1600 RPM. All the welds were produced perpendicularly to the rolling direction for both the alloys. Microhardness (HV) and tensile tests performed at room temperature were used to evaluate the mechanical properties of the joints. The mechanical tests were performed on the joints previously subjected to annealing at 250 °C for 1 h. For the fatigue tests, a resonant electromechanical testing machine was employed under constant loading control up to 250 Hz sine wave loading. The fatigue tests were conducted in the axial total stress–amplitude control mode, with $R = \sigma_{min}/\sigma_{max} = 0.1$. In order to analyse the microstructural evolution of the material, the welds' cross-sections were observed optically and SEM observations were made of the fracture surfaces.

1. Introduction

The friction stir welding (FSW) represents, actually, a new winning technology in the high performance aerospace and automotive application [1]. When compared to traditional welding techniques, FSW strongly reduces the presence of distortions and residual stresses [2–4].

In the friction welding process, joining is done with the help of frictional heat generated at the faying surfaces of the two sheets to be joined with the specially designed rotating tool, which travels down the length of the contacting plates. This produces a highly plastically deformed zone through the associated stirring action. From a forming point of view, the deformation can be described as forging for the tool pressure and advancing and an extrusion along the pin due to its rotation [1]. The localized thermo-mechanical affected zone is produced by friction between the tool shoulder and the plate top surface, as well as by plastic deformation of the material in contact with the tool [5].

The FSW process is a solid state process and therefore a solidification structure is absent in the weld.

The problems related to the presence of brittle inter-dendritic and eutectic phases are eliminated [6].

By developing such technology, one of the most important fact is represented by the possibility of joining different aluminium alloys [7].

Many papers are present in the literature regarding this field. Some authors have demonstrated that the microstructure of the weld nugget of strongly different aluminium alloys is mainly fixed at the retreating side of the material [8]. Murr et al. [9] showed the properties of dissimilar casting alloys by FSW. Also the corrosion susceptibility of dissimilar welds was successfully studied [10]. The microstructural evolution of dissimilar welds as a function of processing parameters has been widely studied in [11], showing the behaviour of AA6061–AA2024 materials.

While extensive studies have been published on dissimilar FSW joints, only very few papers exist regarding the fatigue properties of such kind of weld. Especially with reference to the variation of welding parameters.

This work was aimed at the evaluation of mechanical and microstructural behaviour of AA6082–AA2024 plates obtained by employing different configurations and different FSW parameters.

2. Experimental procedure

The dissimilar AA6082–AA2024 joints were produced using commercial alloys manufactured by Pechiney, in the form of rolled plates of 4 mm thickness (2024 in T3 state and 6082 in the T6 one). Large plates of 200 mm length × 80 mm width were welded perpendicularly to the rolling direction by employing the processing

* Corresponding author. Tel.: +39 0832297324; fax: +39 0832325004.
E-mail address: pasquale.cavaliere@unile.it (P. Cavaliere).

0261-3069/$ - see front matter © 2008 Elsevier Ltd. All rights reserved.
doi:10.1016/j.matdes.2008.05.044

Table 1
Welding conditions employed to join the AA2025–AA6056 plates

Weld	Rotating speed (RPM)	Welding speed (mm/min)
FSW 6082–2024	1600	80
FSW 6082–2024	1600	115
FSW 2024–6082	1600	80
FSW 2024–6082	1600	115

conditions described in Table 1. Such parameters were chosen because for similar base materials, with a revolutionary pitch in the range of 0.07–0.1 [12], the process is performed in the optimal temperature and strain rates conditions to produce good microstructure quality without defects for butt joints and therefore sound welds are achieved. In previous studies, it was observed that for dissimilar alloys it is convenient to decrease the revolutionary pitch [13]. Different materials positioned on the advancing side of the tool allowed four different welding conditions. The treaded C40 steel tool used for the welds was of conical shape with a large diameter of 3.8 mm and small diameter of 2.6 mm, the shoulder diameter measured 9.5 mm.

The machine used for the production of the joints was instrumented with a Kistler three channel load cell in order to record both the forces along the tool axis, hereon denoted as FZ, and along the welding direction, hereon denoted as FX, for all the produced welds. Acquisition scan rate was changed as a function of the processing parameters in order to record two time samples per tool revolution, in all the examined conditions.

Some specimens for the microstructural observations of the cross-sections were prepared by standard metallographic grinding techniques and subsequent electro-polishing (20 s at 20 V in 78 ml of perchloric acid, 120 ml distilled water and 800 ml ethanol solution) and anodizing (90 s at 20 V in 5% fluoboric acid solution) to reveal the grain structure. Light microscopy images allowed a statistical analysis of the nugget area.

The Vickers hardness profiles of all the welded zones were measured on a cross-section perpendicular to the welding direction using a Vickers indenter with a 5 N load for 15 s. In order to evaluate the mechanical properties of the joints obtained in the various welding conditions, tensile tests were performed in a direction transversal to the welding line.

Using an electrical discharge machine (EDM), 200 mm specimens were sectioned with a gauge length of 80 mm and a gauge width of 12.5 mm. Some joints were also annealed at 250 °C for 1 h in order to detect the modifications in the mechanical behaviour. The tensile tests were carried out at room temperature using a MTS 810 testing machine, the cross-head speed is set to 0.1 mm/min, according to the ASTM-E8 standard code, an accurate extensometer of type MTS 634.12 F-24, 25 mm base length, has been used.

Endurance fatigue tests were performed using a resonant electro-mechanical testing machine under constant loading control up to 250 Hz sine wave loading (TESTRONICTM 50 ± 25 kN, produced by RUMUL, SUI) in both low and high regimes, the gauge dimensions of the specimens were 80 mm long and 15 mm wide. The cyclic fatigue tests were conducted up to failure under axial total stress-amplitude control mode under fully reversed, push–pull, tension loading ($R = \sigma_{min}/\sigma_{max} = 0.1$). A FEGSEM (JEOL-JSM 6500 F) was used to study the fracture surfaces of the material after tensile and fatigue tests.

3. Results and discussion

FSW is becoming a very effective tool in solving the joining problems in the aerospace industry, where joints of high ductility and tensile strength are required. In this work, FSW dissimilar welds of AA6082–AA2024 sheets were successfully obtained by varying the processing parameters and the position of the different alloys on the advancing side of the tool (Fig. 1); no superficial defects were detected by macroscopic observations. The different configurations and the processing parameters are indicated in Table 1.

During the initial stage of welding, higher force values act on the material due to tool penetration (F_Z), since the material temperature is still low and consequently its yield strength is high (Fig. 2). Only when the tool penetration is complete and the travel motion has not yet started, the softening of the material induces a drop in the F_Z force. The vertical force increases, as a general behaviour, as increasing the travel speed for all the produced joints

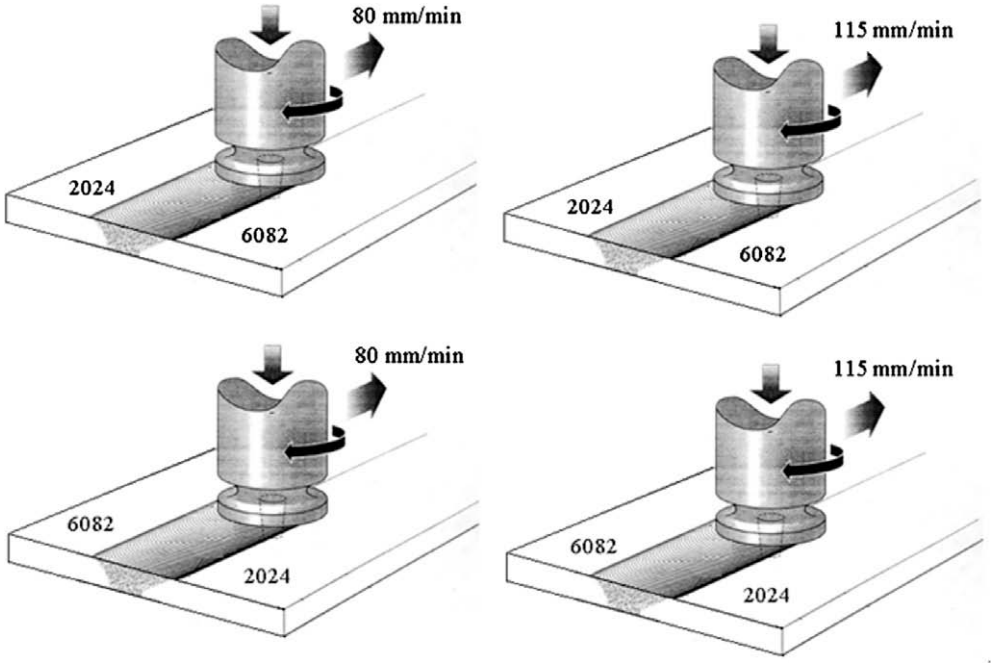

Fig. 1. Schematization of the produced welds in different conditions and with different positions of the alloy plates.

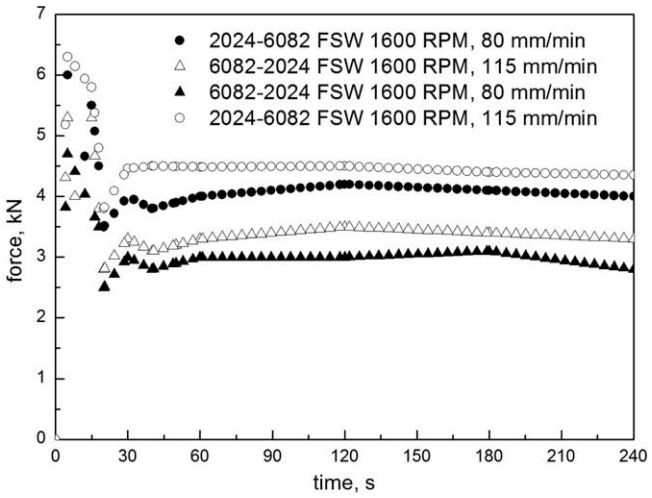

Fig. 2. Vertical forces acting between the tool and the plates in all the welding conditions.

increases. The forces acting on the plates in the case of the higher strength material (AA2024) positioned on the advancing side of the tool resulted higher with respect to the corresponding welds with the softer material (AA6082) positioned in the advancing side.

3.1. Microstructural evolution

The macroscopic aspect of the studied joints is shown in Fig. 3. The cross-section typical feature of the nugget zones of dissimilar aluminium FSW joints is shown in Figs. 4 and 5, (the AA6082 is on the advancing side, left side of the picture). The nugget zones which appeared to be composed of different regions of both the alloys were severely plastically deformed. During FSW, the tool acts as a stirrer extruding the material along the welding direction. Such complex deformation produces the vortex structure composed of alternative lamellae of 2024 and 6082 aluminium alloys. By employing a threaded tool the material is forced from the plate down into the weld and may travel several times depending on the rotational and welding speed. This is the reason for the different vortex structures obtained at different welding conditions. The varying rate of the dynamic recovery or recrystallization is

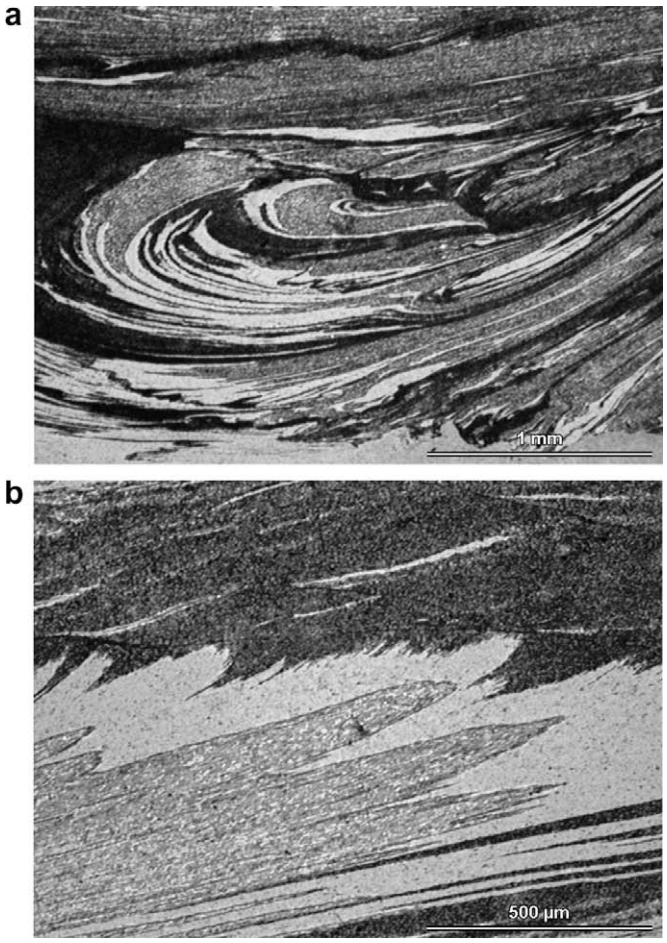

Fig. 4. Microstructure of the joints with AA6082 on the advancing side (115 mm/min) revealing the different nuggets in (a), TMAZ and (b) HAZ at higher magnification.

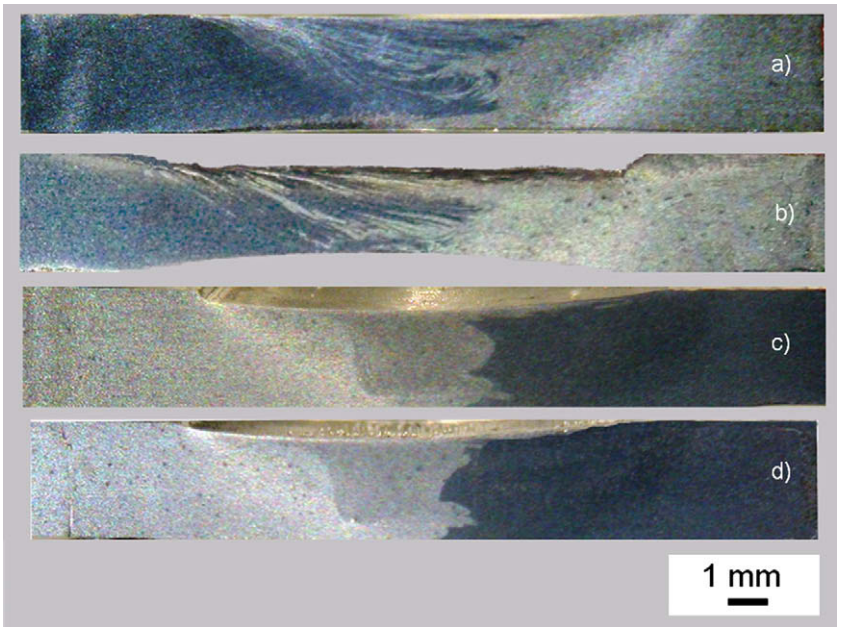

Fig. 3. Macrographs of the studied joints, (a) 2024–6082 80 mm/min, (b) 2024–6082 115 mm/min, (c) 6082–2024 80 mm/min, and (d) 6082–2024 115 mm/min.

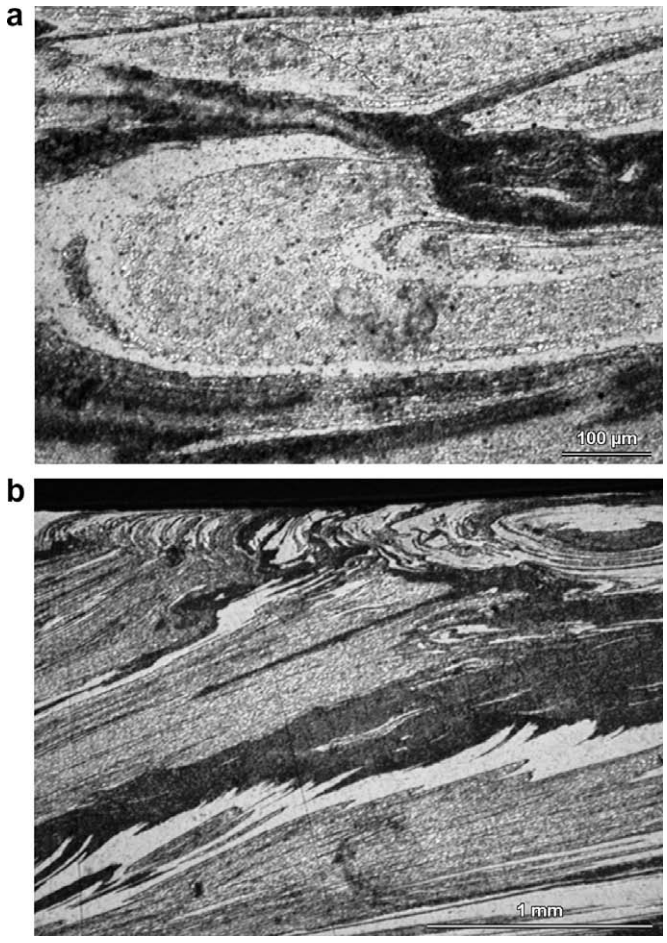

Fig. 5. Microstructure of the joints with AA6082 on the advancing side (80 mm/min a) revealing the different nuggets (a), TMAZ and (b) HAZ at higher magnification.

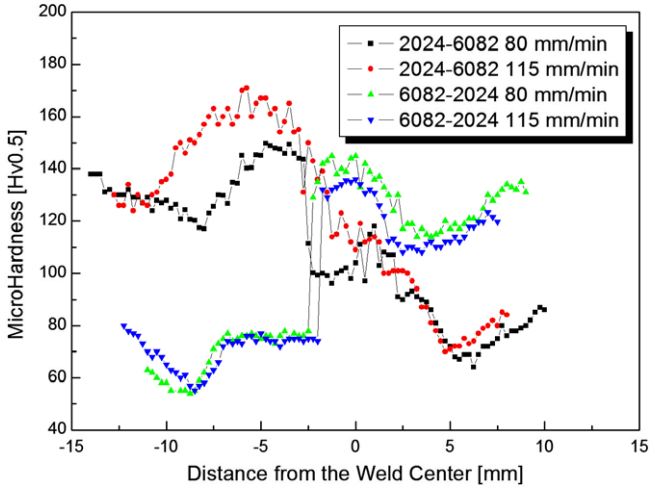

Fig. 6. Microhardness profiles of the studied joints in different conditions.

strongly dependent on the temperature and strain rate reached during deformation. It is also responsible for the different vortex-like structure produced in the center of the welds. Instead, the bonding between different materials is complete in all the welding conditions. Also, it was found that the processing parameters and the material at the advancing side of the tool strongly influence the material mixing.

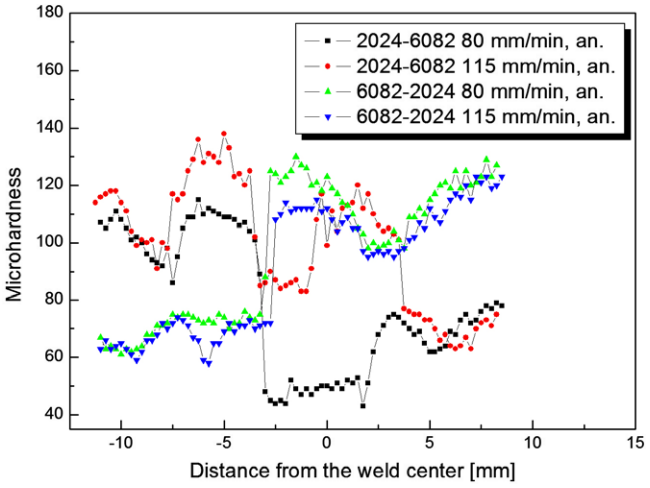

Fig. 7. Microhardness profiles of the studied joints in different conditions after annealing.

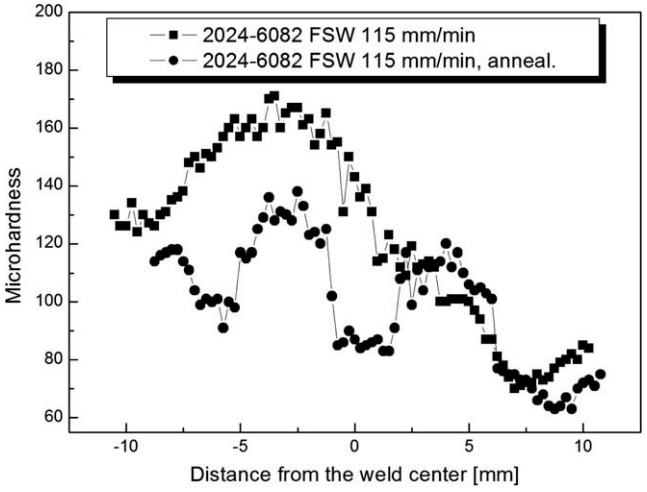

Fig. 8. Comparison of microhardness profiles of the joints welded with AA2024 on the advancing side at 115 mm/min in as-welded and annealed conditions.

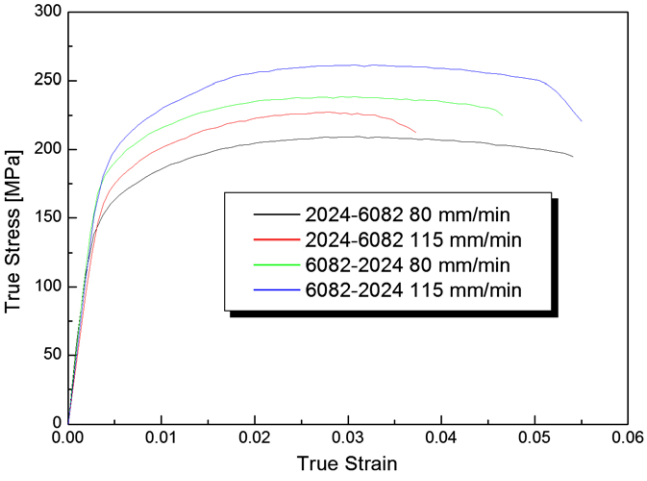

Fig. 9. Tensile properties of the studied joints in different configurations.

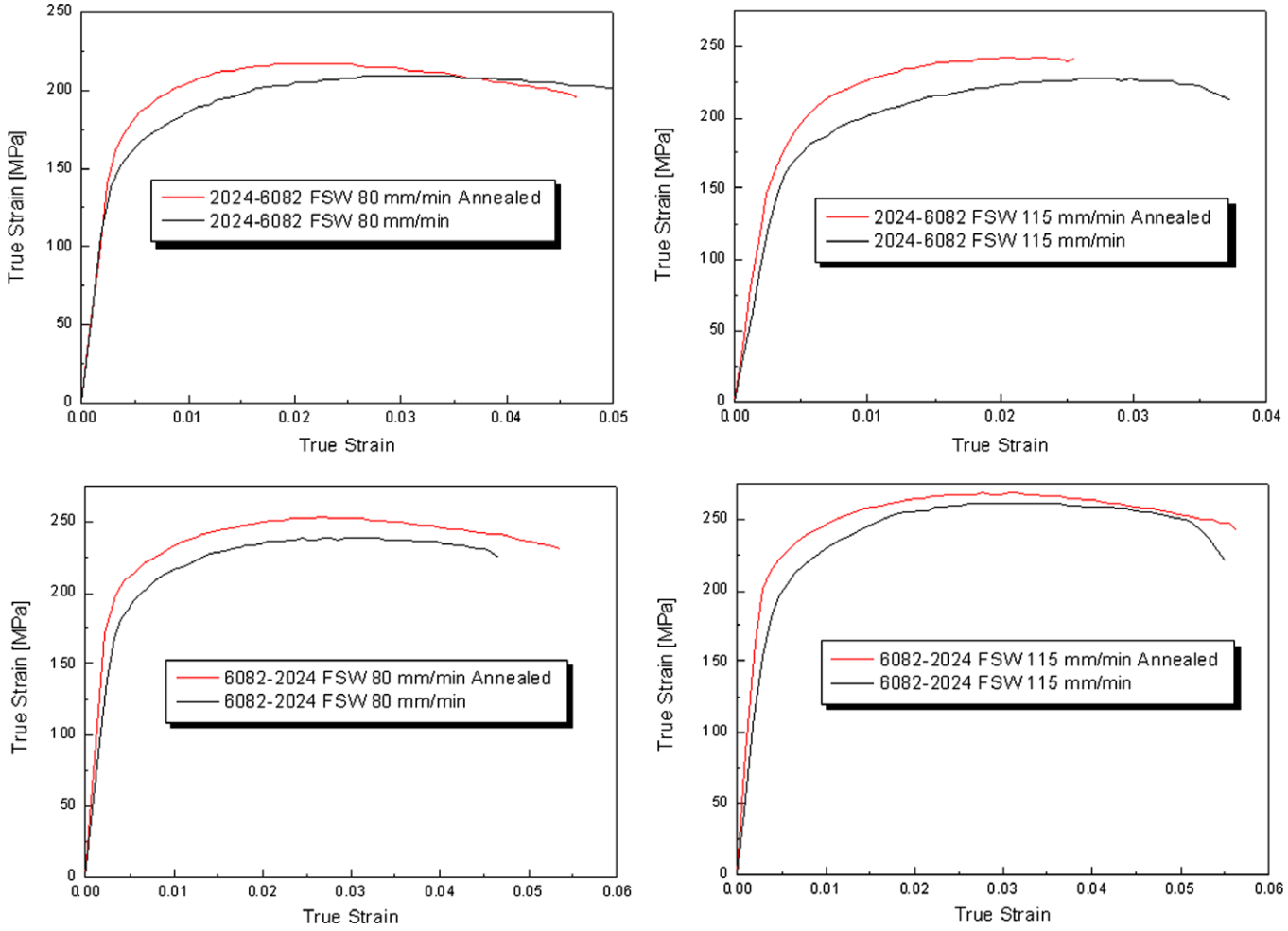

Fig. 10. Tensile properties of the studied joints in different configurations in as-FSW condition compared with those after annealing.

Table 2
Mechanical properties obtained from tensile tests

Material	σ_y (MPa)	UTS (MPa)	ε_f
FSW 2024	275	350	0.058
FSW 6082	245	260	0.09
FSW 6082–2024	200	235	0.14

All the welds were obtained by employing a rotating speed and a welding speed of 1600 RPM and 115 mm/min, respectively.

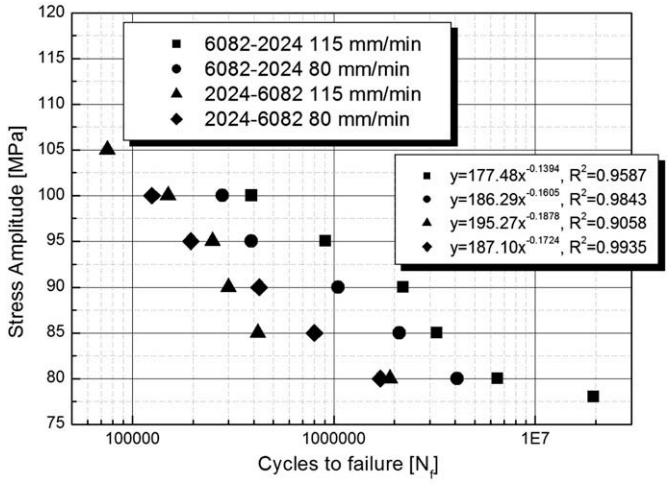

Fig. 11. S–N curves of the dissimilar joints in all the used conditions.

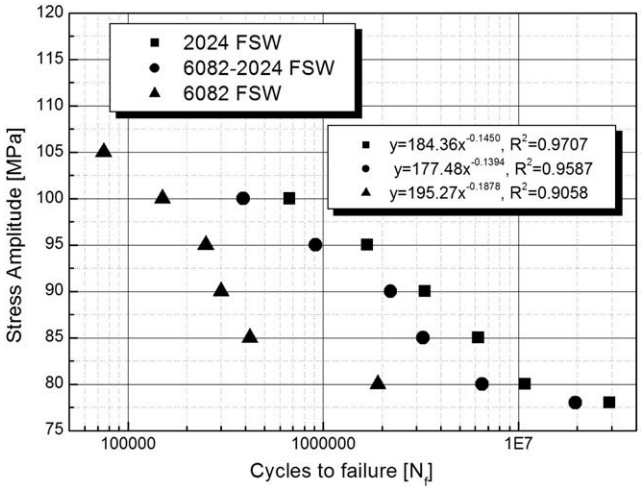

Fig. 12. S–N fatigue curves of the AA6082–AA2024 dissimilar joints compared with the fatigue endurance curves of the AA2024 and AA6082 welds joined by employing the same welding parameters, the slope (R) and the standard deviations (SD) are indicated.

3.2. Mechanical properties

Fig. 6 shows the classical microhardness profiles of dissimilar welds. The highest values of microhardness are reached in the case of dissimilar AA2024–AA6082 when the 2024 alloy is on the

advancing side of the tool and the welding speed is 115 mm/min. When 6082 alloy is employed on the advancing side of the tool, the microhardness profile in the weld nugget appears more uniform, indicating a better mixing of the material. Furthermore, the maximum hardness values in the nugget zone correspond to the welds with AA6082 on the advancing side. In all the cases, the minimum microhardness is reached in the HAZ because of an overaging effect. This is due to the fact that the HAZ has been deformed very slightly, and has different thermo-mechanical behaviour with respect to the nugget and the TMAZ. Some scientists demonstrated such effect by analyzing the reinforcing particles' behaviour in terms of dimension and aspect ratio in the FSW AA6056 alloy by employing a deep transmission electron microscopy analysis [14]. The low microhardness was explained to be due to the disappearance of G.P. zones and formation of overaged precipitates. The slightly higher hardness in the retreating TMAZ is due to a broader temperature gradient resulting in less dissolution and overaging, while The slight increase in hardness of the nugget is related to the complete solution and new precipitation in this slowest cooling zone.

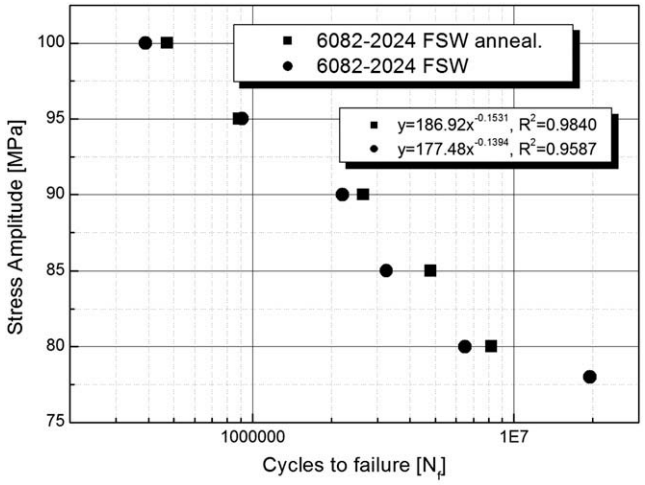

Fig. 13. S–N fatigue curve of AA6082–AA2024 in the as-FSW and annealed conditions, the slope (R) and the standard deviations (SD) are indicated.

The variation of the microhardness values after annealing, is shown in Fig. 7. For all the conditions employed, the values decrease as a consequence of the annealing and the microhardness profile becomes uniform in the vicinity of the retreating side (Fig. 8).

The tensile properties of the dissimilar joints obtained in the various welding conditions is shown in Fig. 9. With the same material on the advancing side, the tensile strength increases by increasing the weld speed of the tool. The ductility is higher with increasing the weld speed in the case of AA6082 on the advancing side, while it decreases in the case of AA2024 on the advancing side. Such dependence of the strength on the material position was previously observed [15]. The best conditions of strength and ductility are reached in the joints welded with AA6082 on the advancing side and an advancing speed of 115 mm/min.

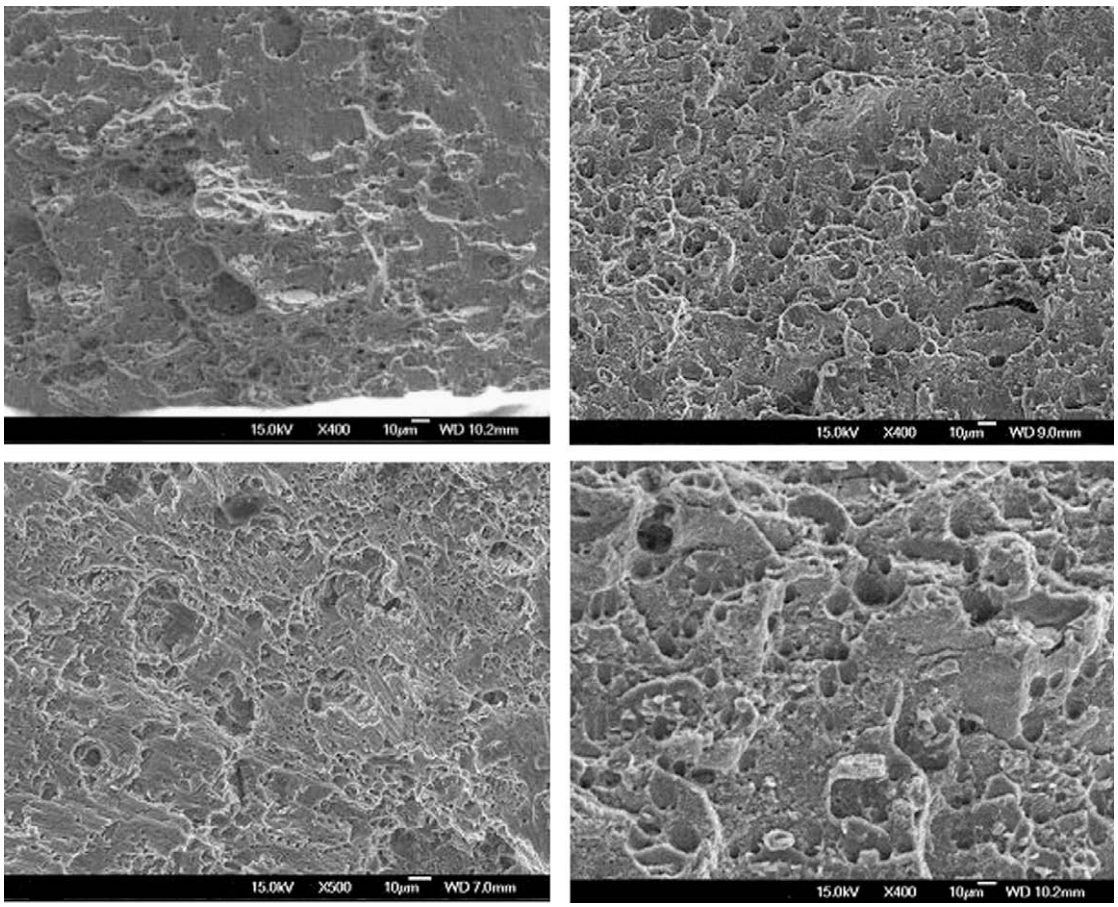

Fig. 14. Fracture surfaces of the tensile tested specimens, respectively: AA2024–AA6082 80 mm/min, AA2024–AA6082 115 mm/min, AA6082–AA2024 80 mm/min, AA6082–AA2024 115 mm/min.

The annealing resulted in a favourable increase in the strength and ductility of the FSW joints, thanks to the residual stresses relaxation (Fig. 10). This behaviour is classical in dissimilar aluminium alloys joints in which the material on the retreating side occupies the larger fraction of the stir zone, due to the different forces acting on the advancing and on the retreating sides [12]. For comparison, in Table 2 the tensile properties of AA2024 and AA6082 joined with the same processing parameters are reported. The joints show lower strength in the dissimilar configuration due to the alternate lamellar structure, but they generally present higher ductility.

The fatigue endurance curve of the dissimilar joints welded in all the studied conditions is shown in Fig. 11.

At a fixed rotating speed, the fatigue behaviour of the dissimilar joints with AA6082 on the advancing side is strongly dependent on the speed of the tool: the fatigue strength increases as the welding speed increases. For the joints obtained with the AA2024 on the advancing side, the welding speed does not influence the fatigue behaviour so strongly.

At the highest stresses and 115 mm/min welding speed, dissimilar FSW joints with AA6082 on the advancing side present a quite similar fatigue life to FSW AA6082, while for lower stresses and higher number of cycles, their behaviour is much closer to that of FSW AA2024 joints (Fig. 12). For 80 MPa stress amplitude, the number of cycles to failure results to be around 2×106 for the AA6082, 1.1×107 for the AA2024 and 6.5×106 for the dissimilar welds. In the AA6082–AA2024 joints, the fracture starts in the advancing side of the tool, where the stress concentration is higher with respect to the retreating side.

The dissimilar as-FSW joints exhibit lower fatigue resistance when compared to the annealed joints. This difference is more marked at the lower stresses (Fig. 13).

3.3. Fractographic behaviour

The SEM observations of the tensile-tested specimens revealed that the failure is in all cases governed by coalescence of microvoids (Fig. 14). SEM observations of the fracture surfaces of the fatigue-tested specimens revealed that at the higher cycles to failure the fatigue cracks initiate and grow along the onion flow lines. In Fig. 15a and b such behaviour is shown for AA6082–AA2024 (115 mm/min) and AA2024–AA6082 (115 mm/min), which failed, respectively, at $N_f = 6.5 \times 106$ $\sigma_a = 80$ MPa and $N_f = 1.9 \times 106$ $\sigma_a = 80$ MPa. As a general result, it can be affirmed that in this stress regime the microstructural feature of the joints is very similar (the crack initiating along the onion flow lines) and the

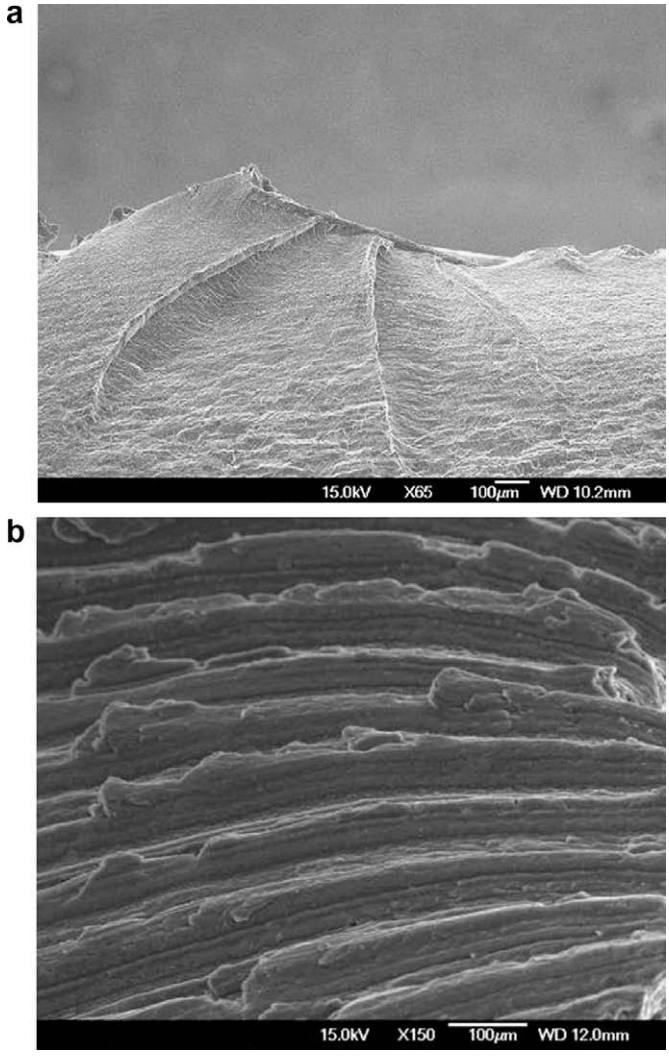

Fig. 15. SEM image of the fracture surface of the dissimilar FSW AA6082–AA2024 (115 mm/min) failed at $N_f = 6.5 \times 106$ $\sigma_a = 80$ MPa (a); and AA2024–AA6082 (115 mm/min) failed at $N_f = 1.9 \times 106$ $\sigma_a = 80$ MPa (b).

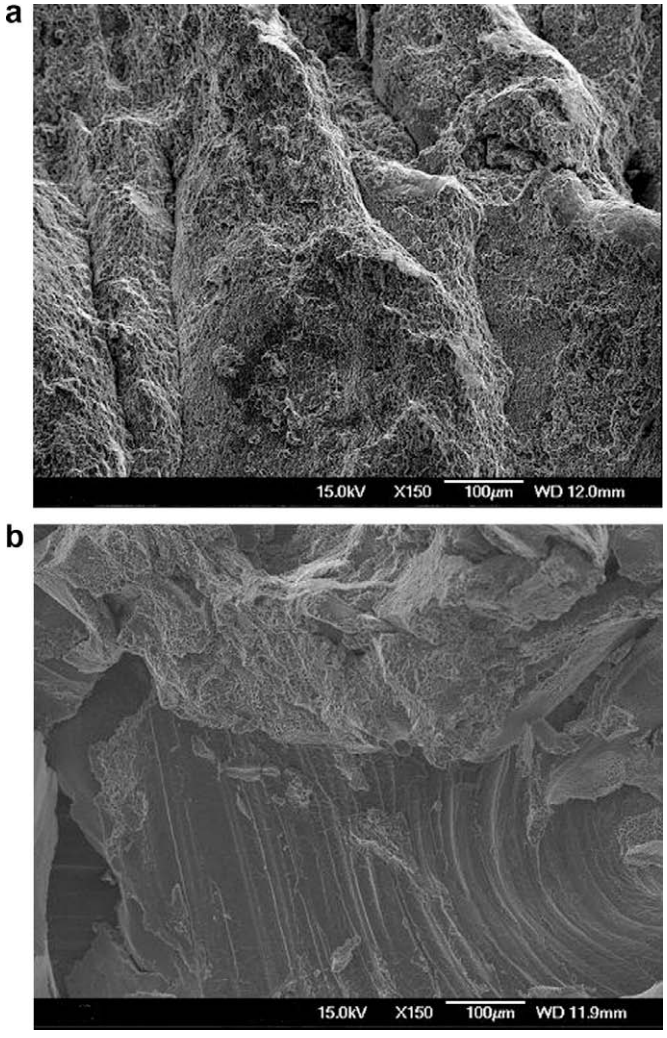

Fig. 16. SEM image of the fracture surface of the dissimilar FSW AA6082–AA2024 (115 mm/min) failed at $N_f = 390{,}000$ $\sigma_a = 100$ MPa (a); and AA2024–AA6082 (115 mm/min) failed at $N_f = 150{,}000$ $\sigma_a = 100$ MPa (b).

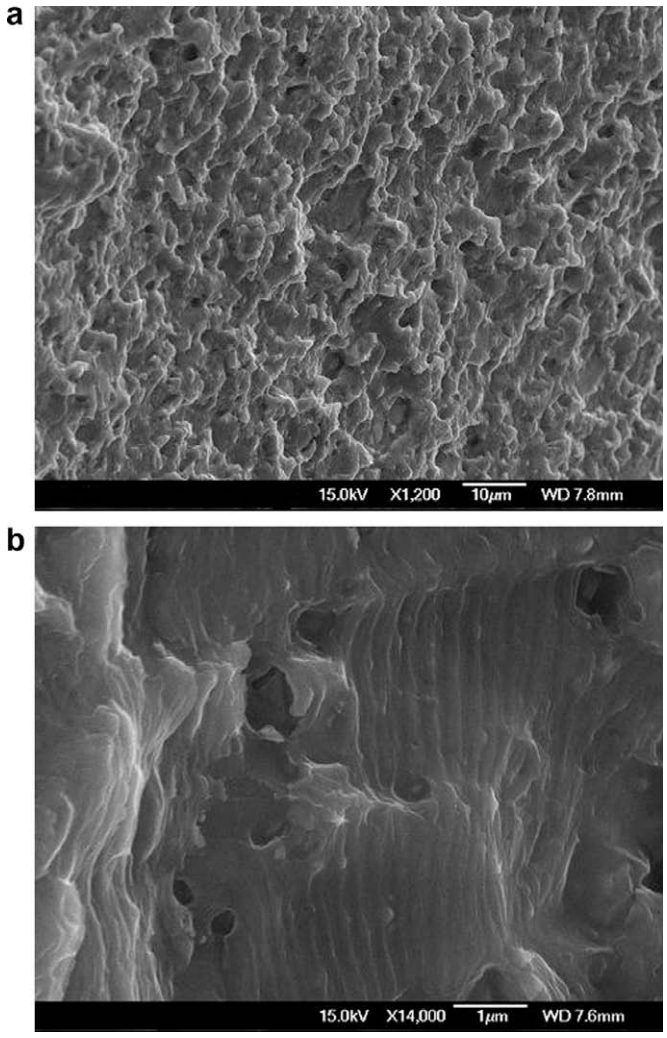

Fig. 17. SEM image of the fracture surface of the dissimilar FSW AA6082–AA2024 (115 mm/min) failed at N_f = 390,000 σ_a = 100 MPa.

material positioned on the advancing side of the tool does not play a fundamental role. On the contrary, by increasing the stress level the mechanical behaviour varies in a much more severe way by changing the processing parameters and the material on the advancing side of the tool (as confirmed by the observation of S–N curves), and by changing such conditions the fracture surfaces also appear strongly different. Other forging defects act as failure sites for the fatigue-tested specimens in the lower stresses regime also (Fig. 16). From higher magnification observations it appears clearly that fatigue failure is governed in all conditions by multiple defects in initiation and growth (Fig. 17). In Fig. 17, the striation-like behaviour typical of the localized microplastic deformation is observed.

4. Conclusions

The mechanical and microstructural behaviour of dissimilar FSW AA6082–AA2024 was studied in this paper. The joints were produced with different alloy positioned on the advancing side of the tool. The joints were realized with a rotation speed of 1600 RPM and by changing the advancing speed from 80 to 115 mm/min. The vertical force was observed to increase as the travel speed for all the produced joints increases. The forces acting on the plates in the case of the higher strength material (AA2024) positioned on the advancing side of the tool resulted higher with respect to the corresponding welds with the softer material (AA6082) positioned in the advancing side.

Different vortex-like structure resulted in the center of the joints in all the different configurations. The best tensile and fatigue properties were obtained for the joints with the AA6082 on the advancing side and welded with an advancing speed of 115 mm/min. The fatigue behaviour of the joints is strongly controlled by the material fixed on the advancing side of the tool at high stress amplitude and the difference is reduced as the loading decreases. For the joints obtained with AA2024 on the advancing side, the welding speed does not influence the fatigue behaviour so strongly. The dissimilar as-FSW joints exhibited lower fatigue resistance when compared to the annealed joints. Such behaviour was confirmed by the observations of the fracture surfaces of the fatigue-tested specimens. In fact, with the 2024 alloy positioned on the advancing side of the tool, the fracture initiation was due to the presence of forging defects in the joints.

References

[1] Mishra RS, Ma ZY. Friction stir welding and processing. Mater Sci Eng 2005;R50:1–78.
[2] Bussu G, Irving PE. The role of residual stress and heat affected zone properties on fatigue crack propagation in friction stir welded 2024–T351 aluminium joints. Int J Fatigue 2003;25:77–88.
[3] John R, Jata KV, Sadananda K. Residual stress effects on near threshold fatigue crack growth in friction stir welded aerospace alloys. Int J Fatigue 2003;25:939–48.
[4] Jata KV, Sankaran KK, Ruschau J. Friction-stir welding effects on microstructure and fatigue of aluminum alloy 7050–T7451. Metall Mater Trans 2000;31A:2181–92.
[5] Guerra M, Schmidt C, McClure JC, Murr LE, Nunes AC. Flow patterns during friction stir welding. Mater Charact 2003;49:95–101.
[6] Rhodes CG, Mahoney MW, Bingel WH. Effects of friction stir welding on microstructure of 7075 aluminium. Scripta Mater 1997;36:69–75.
[7] Cavaliere P, Cerri E, Squillace A. Mechanical response of 2024–7075 aluminium alloys joined by friction stir welding. J Mater Sci 2005;40:3669–76.
[8] Lee WB, Yeon YM, Jung SB. The mechanical properties related to the dominant microstructure in the weld zone of dissimilar formed Al alloy joints by friction stir welding. J Mater Sci 2003;38:4183–91.
[9] Murr LE, Rodriguez NA, Almanza E, Alvarez CJ. Study of friction stir welded A319 and A413 casting alloys. J Mater Sci 2005;40:4307–12.
[10] Bala Srinivasan P, Dietzel W, Zettler R, Dos Santos JF, Sivasan W. Stress corrosion cracking susceptibility of friction stir welded AA7075–AA6056 dissimilar joint. Mater Sci Eng 2005;A392:292–300.
[11] Ouyang JH, Kovacevic R. Material flow and microstructure in the friction stir butt welds of the same and dissimilar aluminium alloys. J Mater Eng Perform 2002;11:51–63.
[12] Cavaliere P, Squillace A, Panella F. Effect of welding parameters on mechanical and microstructural properties of AA6082 joints produced by friction stir welding. J Mater Process Technol 2008;200:364–72.
[13] Cavaliere P, Panella F. Effect of tool position on the fatigue properties of dissimilar 2024–7075 sheets joined by friction stir welding. J Mater Process Technol, in press. doi:10.1016/j.jmatprotec.2007.12.036.
[14] Cabibbo M, McQueen HJ, Evangelista E, Spigarelli S, Di Paola M, Falchero A, et al. Microstructure and mechanical property studies of AA6056 friction stir welded plate. Mater Sci Eng A 2007;460–461:86–94.
[15] Lee Won-Bae, Yeon Yun-Mo, Jung Seung-Boo. The joint properties of dissimilar formed Al alloys by friction stir welding according to the fixed location of materials. Scripta Mater 2003;49:423–8.